

Geometric quench and non-equilibrium dynamics of fractional quantum Hall states

Zhao Liu,¹ Andrey Gromov,² and Zlatko Papić³

¹*Freie Universität Berlin, Dahlem Center for Complex Quantum Systems
and Institut für Theoretische Physik, Arnimallee 14, 14195 Berlin, Germany*

²*Kadanoff Center for Theoretical Physics, University of Chicago, Illinois 60637, USA*

³*School of Physics and Astronomy, University of Leeds, Leeds LS2 9JT, UK*

(Dated: July 22, 2022)

We introduce a quench of the geometry of Landau level orbitals as a probe of non-equilibrium dynamics of fractional quantum Hall (FQH) states. We show that such geometric quenches induce coherent many-body dynamics of neutral degrees of freedom of FQH fluids. The simplest case of mass anisotropy quench can be viewed as a sudden tilt of the magnetic field, and the resulting dynamics reduces to the harmonic motion of the spin-2 “graviton” mode, i.e., the long wavelength limit of the Girvin-MacDonald-Platzman magnetoroton. We derive analytical description of the graviton dynamics using the bimetric theory of FQH states, and find agreement with exact numerical simulations at short times. We show that certain types of geometric quenches excite higher-spin collective modes, thus establishing their existence in a microscopic model and motivating an extension of geometric theories of FQH states.

Introduction.—As a paradigm of strongly correlated systems, fractional quantum Hall (FQH) phases remain in the focus of research due to their remarkable properties such as fractionalization [1], topological order [2], exotic quasiparticles [3, 4] and robust edge excitations [5, 6]. In recent years, a new property has been added to this list: the existence of geometric degrees of freedom that govern the physics of neutral excitations in FQH phases [7–21]. Intriguingly, the neutral degree of freedom is formally reminiscent of a fluctuating space-time metric [22–24]. As it also carries spin-2, this degree of freedom has been dubbed “graviton” [25, 26]. The richness of *topological* properties of FQH phases is therefore further boosted by the collective excitations which have *geometric* character.

In this paper we investigate out-of-equilibrium dynamics of geometric degrees of freedom in FQH phases. In contrast to equilibrium properties of FQH systems at zero temperature, which have been well understood due to a combination of powerful theoretical approaches [1, 3, 4, 27, 28], the dynamics out of equilibrium has received little attention to date. By contrast, in many 1D integrable and critical systems a study of quantum dynamics has provided a wealth of theoretical [29, 30] as well as experimental [31] insights. Here we introduce a theoretical framework for studying FQH phases out of equilibrium, focusing in particular on their neutral bulk excitations.

In order to probe neutral degrees of freedom of FQH states, we introduce *geometric quench* – a sudden change of ambient geometry of a FQH fluid [Fig. 1(a)]. While in integrable systems the term “geometric quench” refers to a sudden change of the size of system [32–35] (e.g., controlled by the trap potential in cold atomic systems), our setup assumes that the size of the FQH system remains fixed, but the geometry of Landau level orbitals undergoes an abrupt change. This geometry can be directly tuned by tilting the magnetic field [36, 37]. As a common experimental technique, tilted field is regularly used

to measure spin polarization of FQH states [38], and has recently been employed to map out the anisotropy of the composite fermion Fermi surface [39].

We demonstrate that geometric quench induces the dynamics of neutral degrees of freedom in FQH states. In the simplest type of quenches driven by the band mass tensor deformation in the Laughlin phase, we show that the post-quench dynamics is a coherent oscillation of the graviton, i.e., the spin-2 excitation in the continuum of the energy spectrum. Furthermore, we show that geometric quench provides a stringent microscopic test of the effective “bimetric” theory of FQH states [23]. We use bimetric theory to analytically obtain the universal *non-linear* equations that govern the post-quench dynamics of geometric degrees of freedom in FQH fluids, Eqs. (4) and (5). We demonstrate that these equations are in agreement with exact numerical simulations of geometric quenches, for moderate times and moderate changes in anisotropy. Finally, we also design more complex types of quenches which excite the higher-spin excitations in the spectrum of FQH states, thus exposing the present limitations of the bimetric theory. We note that higher-spin symmetry has attracted much interest in various areas of theoretical physics [40–45]. The presence of higher spin excitations in FQH states, here unambiguously identified via their distinct dynamical response in a microscopic model, reveals a much richer structure present in FQH states, and calls for an extension of their geometric description beyond the 2×2 unimodular metric [22].

Model.—The Hamiltonian of a FQH system is $H = \sum_{\mathbf{q}} \tilde{V}_{\mathbf{q}} \tilde{\rho}_{\mathbf{q}} \tilde{\rho}_{-\mathbf{q}}$, where $\tilde{V}_{\mathbf{q}}$ and $\tilde{\rho}_{\mathbf{q}}$ are Fourier transforms of the interaction potential and the density operator projected to a single Landau level, respectively [46]. We consider lowest Landau level (LLL) where $\tilde{V}_{\mathbf{q}} = V_{\mathbf{q}} |F_m(\mathbf{q})|^2$, $F_m(\mathbf{q})$ is the LLL form factor and $V_{\mathbf{q}}$ is the Fourier transform of the bare interaction. “Geometry” appears in such a FQH system in three distinct guises. First,

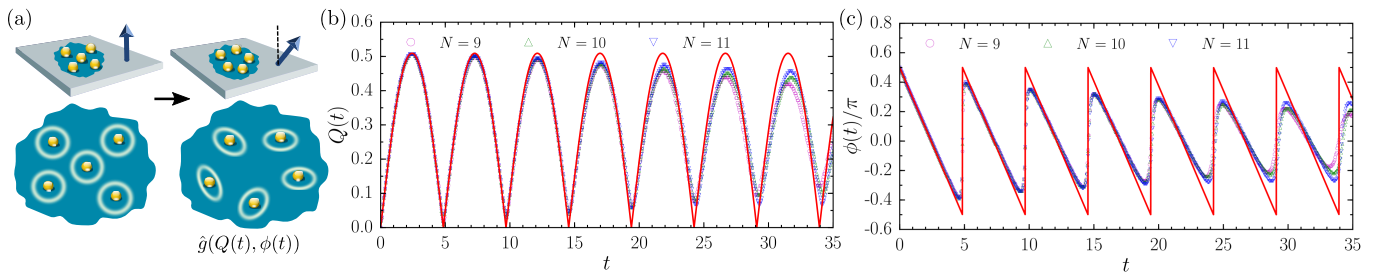


FIG. 1. (a) Geometric quench protocol: sudden tilt of the magnetic field induces dynamics of the intrinsic metric \hat{g} , which describes the shape of particle-flux composites that form a FQH state. (b), (c): Exact dynamics of Q and ϕ for $N = 9 - 11$ bosons at $\nu = 1/2$ with contact interaction. The quench is driven by choosing $A_0 = 0$ and $A_1 = \ln 1.3$. The red curves are fits to Eq. (2), which coincide with the predictions of the bimetric theory.

$F_m(\mathbf{q}) = \exp(-g_m^{ab} q_a q_b \ell_B^2/4)$ is a function of the band mass tensor g_m , where ℓ_B denotes the magnetic length. This tensor can be conveniently parametrized by a 2×2 unimodular matrix, e.g.,

$$g_m = \begin{pmatrix} \cosh Q + \cos \phi \sinh Q & \sin \phi \sinh Q \\ \sin \phi \sinh Q & \cosh Q - \cos \phi \sinh Q \end{pmatrix}, \quad (1)$$

where Q and ϕ are real numbers which parametrize a stretch or rotation (note, $\det g_m = 1$). Second, $V_{\mathbf{q}}$ in general depends on another rank-2 tensor g_i , characterizing the underlying solid state material (g_i originates from the dielectric tensor of the material for the Coulomb interaction). Both g_m and g_i are set by *extrinsic* experimental conditions. Subject to these two extrinsic tensors, a FQH state develops a third, *intrinsic* geometric degree of freedom. This intrinsic degree of freedom defines the shape of particle-flux composite droplets in the FQH state and can be thought of as a metric \hat{g} , which is similarly parametrized by an analog of Eq. (1). Intrinsic metric \hat{g} is a “compromise” between g_m and g_i [47], because g_m and g_i are physically independent and in general different from each other. The dynamics of \hat{g} can be induced by tilting the magnetic field [Fig. 1(a)], which can be exactly modelled by 2×2 anisotropic mass tensor for parabolic confining potential [36, 37, 47]. This forms the key component of the geometric quench protocol.

Quench protocol.—For concreteness, we focus on bosons on a square torus at filling factor $\nu = 1/2$, interacting via short-range contact potential whose Fourier transform is $V_{\mathbf{q}} = 1$ (similar results are obtained for Coulomb potential and fermionic particles [48]). In this case, the bosons form an incompressible Laughlin state [1], with one boson per area corresponding to two magnetic fluxes [Fig. 1(a)]. Geometric quench can now be defined as follows. (i) At time $t = 0$, we prepare a Laughlin state $|\psi_0\rangle$ as the ground state of H with some mass tensor g_m . (ii) We instantaneously change $g_m \rightarrow g'_m$, assuming for simplicity that both are diagonal, i.e., $g_m = \text{diag}(e^{A_0}, e^{-A_0})$ and $g'_m = \text{diag}(e^{A_1}, e^{-A_1})$. Furthermore, we assume that the equilibrium system is in the Laughlin phase for both g_m and g'_m . Note that g_m and g'_m are not necessarily in-

finitesimally close to each other. (iii) We evolve in time with the quenched Hamiltonian H' , assuming the system is closed, i.e., $|\psi(t)\rangle = \exp(-iH't)|\psi_0\rangle$. Time evolution is computed numerically via exact diagonalization of H' or via Lanczos algorithm in larger system sizes. (iv) We measure the intrinsic metric as a function of time, $\hat{g}(t)$. This is accomplished by the brute force search over a large set of (precomputed) trial states $|\psi_{\text{trial}}\rangle$, i.e., Laughlin wave functions parametrized by $Q \in [0, Q_{\text{max}} = 1]$ and $\phi \in [-\pi, \pi]$, such that the overlap $|\langle \psi_{\text{trial}} | \psi(t) \rangle|$ is maximized. The confidence in the result is quantified by the maximum overlap achieved: if this overlap is not close to 1, none of the trial states appropriately describes the system and the intrinsic metric should be determined via some other means, for example via minimization of the total energy or momentum polarization [49]. While more realistic generalizations of this setup are possible [48], this minimal protocol already yields intricate quantum dynamics.

Results.— We performed numerical simulations of geometric quenches to determine the equation of motion for $\hat{g}(Q, \phi)$. We illustrate this with the simple case where the initial state is the isotropic Laughlin state ($A_0 = 0$), and the quench is driven by $A_1 = \ln 1.3$, i.e., about 30% change in anisotropy. Exact dynamics of \hat{g} is shown in Figs. 1(b),(c). We have found similar results for changes in anisotropy up to 50%.

We observe that both Q and ϕ oscillate with a well-defined frequency, and ϕ is a *linear* function of time. The existence of such coherent oscillations in \hat{g} is surprising because a 30% change in anisotropy couples the ground state to the continuum of excited states in the energy spectrum, which normally would lead to a rapid decay of oscillations. In order to understand the coherent dynamics with a well-defined frequency, we first observe that the oscillations in Figs. 1(b),(c) are well described by a single harmonic

$$Q(t) = \pm 2A \sin\left(\frac{E_{\gamma} t}{2}\right), \quad \phi(t) = \pi \mp \frac{\pi}{2} - \frac{E_{\gamma} t}{2}. \quad (2)$$

Note that only one of these two solutions is independent

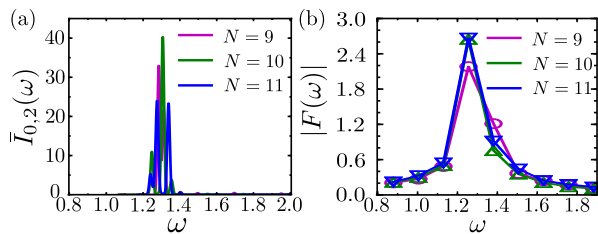


FIG. 2. (a) Normalized spectral function $\bar{I}_{0,2}(\omega)$ for isotropic systems of $N = 9 - 11$ bosons at $\nu = 1/2$ with contact interaction. (b) Discrete Fourier transform $|F(\omega)|$ of Q in Fig. 1(b).

because the system is invariant under $Q \rightarrow -Q$ and $\phi \rightarrow \phi + \pi$. Thus, we can focus on the $Q \geq 0$ part and consider $\phi \bmod 2\pi$. By inspection of $Q(t)$, we see the solution will alternate between the two branches, which doubles the frequency from $E_\gamma/2$ to E_γ . The overall prefactor (written as $2A$) is expected to be proportional to the anisotropy of H' .

Graviton oscillation.—Fitting the first one or two oscillations in Figs. 1(b),(c) against Eq. (2) indeed yields a remarkably accurate agreement with full dynamics across the entire time interval. What is the physical origin of the oscillations and what sets the frequency, E_γ ? From the fits, we obtain $E_\gamma \approx 1.296$. This value does not match the spectral gap in the $\mathbf{k} = 0$ momentum sector, which is only about 1.08. Instead, as we now show, this estimate agrees well with the *graviton* gap, which we independently determine to be 1.3 for the present case.

To justify the identification of E_γ with the graviton gap, we introduce the spectral function $I_{0,2}(\omega) = \sum_j \delta(\omega - \epsilon_j) |\langle j | \hat{V}_{0,2} | 0 \rangle|^2$, where $V_{0,2}$ is the quadrupolar generalization of the Haldane pseudopotential [50] and $|j\rangle$ is an eigenstate with energy ϵ_j . We expect peaks of $I_{0,2}(\omega)$ at energies corresponding to spin-2 excitations that comprise the graviton mode. In Fig. 2, we show the normalized $\bar{I}_{0,2}(\omega) \equiv I_{0,2}(\omega) / \int I_{0,2}(\omega) d\omega$ for an isotropic system (similar data are obtained for weakly anisotropic systems). We observe a sharply pronounced peak of $\bar{I}_{0,2}(\omega)$ around $\omega = 1.3$ for various system sizes, which means that spin-2 eigenstates concentrate in this narrow energy window corresponding to the graviton gap. As an independent estimate of the graviton gap, we use the discrete Fourier transform of Q , Fig. 2(b). This Fourier transform also shows a peak around the same energy as $I_{0,2}(\omega)$, which further confirms that the dynamics of the intrinsic metric is indeed caused by the graviton oscillation. The sharpness of the spectral function reflects the fact only a vanishing fraction of all states in the Hilbert space participate in the post-quench dynamics, as can be confirmed by explicit finite-size scaling [48].

Quench in the bimetric theory.—We now demonstrate that the geometric quench allows us to directly test the bimetric theory of FQH states [23]. Bimetric theory was formulated to describe gapped dynamics of a single spin-2

degree of freedom in a FQH system – the long-wavelength limit of the Girvin-MacDonald-Platzman neutral excitation [7], interacting with an external electro-magnetic field and ambient geometry. The dynamical degree of freedom is the vielbein \hat{e}_i^α [51] that “squares” to the intrinsic metric $\hat{g}_{ij} = \hat{e}_i^\alpha \hat{e}_j^\beta \delta_{\alpha\beta}$. The inverse metric is given by $\hat{G}^{ij} = \hat{E}_\alpha^i \hat{E}_\beta^j \delta^{\alpha\beta}$, where \hat{E}_α^i is the inverse vielbein, satisfying $\hat{E}_\alpha^i \hat{e}_j^\alpha = \delta_j^i$. The unimodular condition on \hat{g}_{ij} reads $\sqrt{g} = \sqrt{\hat{g}}$, where \sqrt{g} is the determinant of the ambient metric g_{ij} . Quadrupolar anisotropy is introduced by modifying the ambient metric, $g_{ij}^m = m_{AB} e_i^A e_j^B$, where e_i^A are the vielbeins that describe the ambient geometry (we assume ambient space is flat, i.e., $e_i^A = \delta_i^A$) and m_{AB} is a unimodular matrix, assumed to be of the form $\text{diag}[e^A, e^{-A}]$, where A is the effective anisotropy.

In a homogeneous magnetic field, the Lagrangian is [23]

$$\mathcal{L} = \frac{\nu\varsigma}{2\pi\ell_B^2} \hat{\omega}_0 - \frac{m}{2} \left(\frac{1}{2} \hat{g}^{ij} g_{ij}^m - \gamma \right)^2, \quad (3)$$

where $\hat{\omega}_0 = \frac{1}{2} \epsilon_{\alpha\beta} \hat{E}_\beta^i \partial_0 \hat{e}_i^\alpha$ is the temporal component of the (dynamic) Levi-Civita spin connection. The phenomenological coefficient m sets the energy scale which determines the gap of the spin-2 mode, $E_\gamma = 2\Omega(1 - \gamma)$, where $\Omega = (m/\varsigma)(2\pi\ell_B^2/\nu)$, and the quantized coefficient ς is determined by the “shift” [23]. Parameter γ is used to tune the theory close to the nematic phase transition in the gapped phase $\gamma < 1$, where the SMA is exact.

In order to compute the dynamics of \hat{g} , we parametrize it in terms of Q and ϕ as in Eq. (1). Both Q and ϕ are functions of time but not space, since we consider global (homogeneous) quench. The equations for $\phi(t)$ and $Q(t)$ can be shown to take the form [48]

$$\begin{aligned} \dot{\phi} \sinh Q &= -2\Omega (\sinh A \cosh Q \cos \phi - \cosh A \sinh Q) \\ &\quad \times (\gamma + \sinh A \sinh Q \cos \phi - \cosh A \cosh Q), \quad (4) \\ \dot{Q} \sinh Q &= -2\Omega \sin \phi \sinh Q \sinh A \\ &\quad (\gamma + \sinh A \sinh Q \cos \phi - \cosh A \cosh Q). \quad (5) \end{aligned}$$

These complicated non-linear equations provide universal description of the neutral dynamics of FQH states. When anisotropy is weak, we can assume both A and Q are close to 0. By Taylor expanding Eqs. (4) and (5) in A and Q [48], it can be shown that for a particular initial condition $Q(0) = 0$, the analytical solution is given by Eq. (2). Thus, the agreement between numerically exact quench dynamics in Figs. 1(b),(c) and Eq. (2) validates the prediction of the bimetric theory. Such an agreement, which we observe as long as we are in the regime where the state before and after the quench remains in the Laughlin phase, is due to an exponentially vanishing fraction of eigenstates that contribute to the dynamics [48], which justifies the fundamental assumption of the bimetric theory about the single spin-2 degree of freedom. Moreover, the fits allow us to extract

the values of A and E_γ , which can now be interpreted as the effective anisotropy and graviton gap. Indeed, the obtained E_γ is found to be insensitive to the precise values of A_0 and A_1 . On the other hand, A quantifies the effective anisotropy in the ground state of H' , for which we expect $A = A_1$ in the present case. Indeed, we get $A \approx 0.255$ from the fit in Fig. 1, which is very close to $A_1 = \ln 1.3 \approx 0.262$.

Dynamics of higher spin modes.—Geometric quench allows us to further explore dynamical effects that are not captured by the bimetric theory. Some of these can be noticed at late times in Fig. 1 as a departure from simple harmonic motion. A possible explanation for this is that the effective spin-2 degree of freedom does not correspond to a single but several many-body eigenstates with similar energies. This “fragmentation” of the graviton mode would induce dephasing in the quench dynamics. A different source of non-trivial dynamics are the higher spin modes, which are not accounted for by the bimetric theory. These modes can be viewed as higher angular momentum distortions of a FQH fluid which preserve its area [52, 53]. Such deformations form the (infinite-dimensional) W_∞ algebra [54, 55], which has appeared in numerous theoretical descriptions of FQH problems [56–60]. While linearized higher spin excitations naturally appear in the vicinity of the composite fermion Fermi liquid state [53, 61], their theoretical significance or the physical consequences in other FQH phases, including the Laughlin phase, are not understood.

Using geometric quench, we can demonstrate that higher spin modes are present even in the simplest Laughlin phases, and leave distinct signatures in the quench dynamics beyond the bimetric theory. We will concentrate on the spin-4 mode, and expose its dynamics by slightly redefining the quench protocol. We first prepare an exact (isotropic) Laughlin state, and then modify the interaction $H \rightarrow H + 0.1\hat{V}_{0,4}$ by adding a small component of *octupolar* pseudopotential, $V_{0,4}$ [50]. This type of quench is relevant for systems whose Fermi contours are not simple ellipses [62, 63]. Surprisingly, for such a quench we find $Q(t) \equiv 0$ during the entire measured time interval, while the quantum fidelity, $|\langle\psi(t)|\psi(0)\rangle|^2$, visibly oscillates, as shown in Fig. 3(a). Instead, if we perform the quench by adding $\hat{V}_{0,2}$, both $Q(t)$ and fidelity oscillate with the same frequency as found above [48].

The failure of the bimetric theory to capture the quench dynamics driven by $\hat{V}_{0,4}$ strongly suggests that this quench is dominated by higher-spin collective modes. Indeed, the spin-4 character of the mode is explicitly confirmed by evaluating the spectral function $\bar{I}_{0,4}(\omega)$ in Fig. 3(b) (with identical results obtained for the discrete Fourier transform, shown in the inset). $\bar{I}_{0,4}(\omega)$ shows two peaks, one of which corresponds to the graviton energy and an additional one at higher energy, $\omega \sim 1.7$, which we identify with the spin-4 mode. This provides an unambiguous example in which the 2×2 unimodular metric

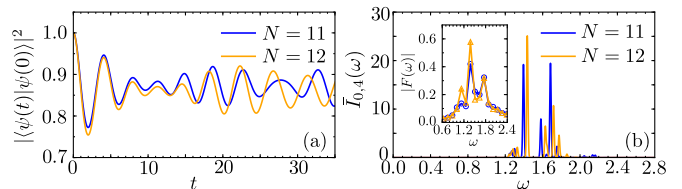


FIG. 3. (a) Exact dynamics of quantum fidelity, $|\langle\psi(t)|\psi(0)\rangle|^2$, for the quench $H \rightarrow H + 0.1\hat{V}_{0,4}$. (b) Normalized spectral function $\bar{I}_{0,4}(\omega)$ for isotropic systems of bosons at $\nu = 1/2$ with contact interaction. Inset shows the discrete Fourier transform $|F(\omega)|$ of (a).

in Eq. (1) is inadequate to fully capture the dynamics in the Laughlin phase, motivating the generalization of the effective geometric theories of FQH states.

Experimental considerations.—While tilted magnetic field is a common technique in FQH experiments, observing coherent dynamics in solid-state materials that host FQH states is challenging: assuming magnetic fields ~ 10 T, the time scale for resolving the graviton oscillation is only $\sim 10^{-14}$ s. Further challenge is measuring the intrinsic metric in gapped FQH states [64], despite recent progress on detecting the anisotropy of the composite fermion Fermi surface [39, 65, 66]. Fortunately, our results directly generalize [48] to lattice FQH systems [67–70], which allow to observe time scales $\sim 10^{-5}$ s (assuming the interaction strength in cold-atom settings is in the order of $2\pi\hbar \times 10$ kHz), which is well within limits of recent experiments [71].

Conclusions.—We have introduced geometric quench as a method for studying the non-equilibrium dynamics of geometric degrees of freedom of FQH states. For certain types of quenches, we have demonstrated an agreement between numerical simulations of exact dynamics and the bimetric theory, which allowed us to obtain universal analytical description of such dynamics in strongly-interacting topological phases. We have also proposed a different type of quench that identifies the enigmatic higher spin modes in the spectrum of Laughlin states, whose dynamics cannot be described by the currently available geometric theories of the FQH effect. The tool of geometric quench allows to explore several new questions about out-of-equilibrium properties of FQH states: (i) what types of dynamical behaviours could arise in FQH states with multiple collective modes, such as multilayer states [72, 73] and non-Abelian states [4], which are known to host exotic neutral excitations [74, 75] beyond the simple SMA description; (ii) how to describe non-linear quench regimes, e.g., the vicinity of the nematic phase transition [76], or quenches across the transition from one FQH phase into another; (iii) what is the quench dynamics of gapless states, such as the composite fermion Fermi liquid; (iv) what types of quench dynamics can occur in lattice FQH systems beyond integer Chern insulators [77, 78], e.g., in higher Chern bands [79–81];

(v) how to generalize the bimetric theory to include a tower of interacting higher spin fields [23, 61, 82], in a way which is consistent with the non-linear structure of W_∞ algebra, that would fully characterize the dynamics after the quench.

Acknowledgements.—We thank V. Caudrelier for illuminating discussions about the system of differential equations. This work was supported in part by the Department of Energy, Office of Basic Energy Sciences through Grant No. DE – SC0002140. Z.L. was supported by Alexander von Humboldt Research Fellowship for Postdoctoral Researchers. A.G. was supported by the Leo Kadanoff fellowship, the NSF grant DMR-1206648, and by the University of Chicago Materials Research Science and Engineering Center, which is funded by the National Science Foundation under award No. DMR-1420709. Z.P. acknowledges support by EPSRC grant EP/P009409/1. Statement of compliance with EPSRC policy framework on research data: This publication is theoretical work that does not require supporting research data.

-
- [1] R. B. Laughlin, *Phys. Rev. Lett.* **50**, 1395 (1983).
 [2] X. G. Wen, *Int. J. Mod. Phys. B* **04**, 239 (1990).
 [3] J. K. Jain, *Phys. Rev. Lett.* **63**, 199 (1989).
 [4] G. Moore and N. Read, *Nuclear Physics B* **360**, 362 (1991).
 [5] B. I. Halperin, *Phys. Rev. B* **25**, 2185 (1982).
 [6] X. Wen, *Modern Physics Letters B* **05**, 39 (1991).
 [7] S. M. Girvin, A. H. MacDonald, and P. M. Platzman, *Phys. Rev. Lett.* **54**, 581 (1985).
 [8] J. E. Avron, R. Seiler, and P. G. Zograf, *Phys. Rev. Lett.* **75**, 697 (1995).
 [9] N. Read, *Phys. Rev. B* **79**, 045308 (2009).
 [10] F. D. M. Haldane, ArXiv e-prints (2009), [arXiv:0906.1854 \[cond-mat.str-el\]](https://arxiv.org/abs/0906.1854).
 [11] J. Maciejko, B. Hsu, S. A. Kivelson, Y. Park, and S. L. Sondhi, *Phys. Rev. B* **88**, 125137 (2013).
 [12] Y. You, G. Y. Cho, and E. Fradkin, *Phys. Rev. X* **4**, 041050 (2014).
 [13] F. Ferrari and S. Klevtsov, *Journal of High Energy Physics* **2014**, 86 (2014).
 [14] A. G. Abanov and A. Gromov, *Phys. Rev. B* **90**, 014435 (2014).
 [15] M. R. Douglas and S. Klevtsov, *Communications in Mathematical Physics* **293**, 205 (2009).
 [16] A. Gromov, G. Y. Cho, Y. You, A. G. Abanov, and E. Fradkin, *Phys. Rev. Lett.* **114**, 016805 (2015).
 [17] B. Bradlyn and N. Read, *Phys. Rev. B* **91**, 125303 (2015).
 [18] T. Can, M. Laskin, and P. Wiegmann, *Phys. Rev. Lett.* **113**, 046803 (2014).
 [19] S. Klevtsov and P. Wiegmann, *Phys. Rev. Lett.* **115**, 086801 (2015).
 [20] T. L. Hughes, R. G. Leigh, and E. Fradkin, *Phys. Rev. Lett.* **107**, 075502 (2011).
 [21] A. Gromov and A. G. Abanov, *Phys. Rev. Lett.* **113**, 266802 (2014).
 [22] F. D. M. Haldane, *Phys. Rev. Lett.* **107**, 116801 (2011).
 [23] A. Gromov and D. T. Son, *Phys. Rev. X* **7**, 041032 (2017).
 [24] P. Wiegmann, *Phys. Rev. Lett.* **120**, 086601 (2018).
 [25] B. Yang, Z.-X. Hu, Z. Papić, and F. D. M. Haldane, *Phys. Rev. Lett.* **108**, 256807 (2012).
 [26] S. Golkar, D. X. Nguyen, and D. T. Son, *Journal of High Energy Physics* **2016**, 21 (2016).
 [27] F. D. M. Haldane and E. H. Rezayi, *Phys. Rev. Lett.* **54**, 237 (1985).
 [28] S. C. Zhang, T. H. Hansson, and S. Kivelson, *Phys. Rev. Lett.* **62**, 82 (1989).
 [29] F. H. L. Essler and M. Fagotti, *Journal of Statistical Mechanics: Theory and Experiment* **2016**, 064002 (2016).
 [30] P. Calabrese and J. Cardy, *Journal of Statistical Mechanics: Theory and Experiment* **2016**, 064003 (2016).
 [31] T. Kinoshita, T. Wenger, and D. S. Weiss, *Nature* **440**, 900 (2006).
 [32] F. Heidrich-Meisner, M. Rigol, A. Muramatsu, A. E. Feiguin, and E. Dagotto, *Phys. Rev. A* **78**, 013620 (2008).
 [33] H. Buljan, R. Pezer, and T. Gasenzer, *Phys. Rev. Lett.* **100**, 080406 (2008).
 [34] J. Mossel, G. Palacios, and J.-S. Caux, *Journal of Statistical Mechanics: Theory and Experiment* **2010**, L09001 (2010).
 [35] V. Alba and F. Heidrich-Meisner, *Phys. Rev. B* **90**, 075144 (2014).
 [36] Z. Papić, *Phys. Rev. B* **87**, 245315 (2013).
 [37] B. Yang, C. H. Lee, C. Zhang, and Z.-X. Hu, *Phys. Rev. B* **96**, 195140 (2017).
 [38] J. P. Eisenstein, R. Willett, H. L. Stormer, D. C. Tsui, A. C. Gossard, and J. H. English, *Phys. Rev. Lett.* **61**, 997 (1988).
 [39] D. Kamburov, Y. Liu, M. Shayegan, L. N. Pfeiffer, K. W. West, and K. W. Baldwin, *Phys. Rev. Lett.* **110**, 206801 (2013).
 [40] A. Dhar, G. Mandal, and S. R. Wadia, *Modern Physics Letters A* **07**, 3129 (1992).
 [41] A. Jevicki and B. Sakita, “The quantum collective field method and its application to the planar limit,” in *The Large N Expansion in Quantum Field Theory and Statistical Physics*, pp. 402–418.
 [42] S. Giombi, I. R. Klebanov, and A. A. Tseytlin, *Phys. Rev. D* **90**, 024048 (2014).
 [43] G. A. Goldin, R. Menikoff, and D. H. Sharp, *Phys. Rev. Lett.* **58**, 2162 (1987).
 [44] V. I. Arnold and B. A. Khesin, *Annual Review of Fluid Mechanics* **24**, 145 (1992).
 [45] I. Bars, *Physics Letters B* **245**, 35 (1990).
 [46] R. Prange and S. Girvin, *The Quantum Hall effect*, Graduate texts in contemporary physics (Springer-Verlag, 1987).
 [47] B. Yang, Z. Papić, E. H. Rezayi, R. N. Bhatt, and F. D. M. Haldane, *Phys. Rev. B* **85**, 165318 (2012).
 [48] Supplemental Online Material.
 [49] A. Gromov, S. D. Geraedts, and B. Bradlyn, *Phys. Rev. Lett.* **119**, 146602 (2017).
 [50] B. Yang, Z.-X. Hu, C. H. Lee, and Z. Papić, *Phys. Rev. Lett.* **118**, 146403 (2017).
 [51] S. Carroll and S. Carroll, *Spacetime and Geometry: An Introduction to General Relativity* (Addison Wesley, 2004).
 [52] A. Cappelli and E. Randellini, *Journal of High Energy Physics* **2016**, 105 (2016).

- [53] S. Golkar, D. X. Nguyen, M. M. Roberts, and D. T. Son, *Phys. Rev. Lett.* **117**, 216403 (2016).
- [54] S. M. Girvin, A. H. MacDonald, and P. M. Platzman, *Phys. Rev. B* **33**, 2481 (1986).
- [55] A. Cappelli, C. A. Trugenberger, and G. R. Zemba, *Nuclear Physics B* **396**, 465 (1993).
- [56] L. Susskind, arXiv preprint hep-th/0101029 (2001).
- [57] A. P. Polychronakos, *Journal of High Energy Physics* **2001**, 011 (2001).
- [58] S. Hellerman and M. V. Raamsdonk, *Journal of High Energy Physics* **2001**, 039 (2001).
- [59] S. Iso, D. Karabali, and B. Sakita, *Physics Letters B* **296**, 143 (1992).
- [60] N. Read, *Phys. Rev. B* **58**, 16262 (1998).
- [61] D. X. Nguyen, A. Gromov, and D. Thanh Son, ArXiv e-prints (2017), arXiv:1712.08169 [cond-mat.str-el].
- [62] F. D. M. Haldane and Y. Shen, ArXiv e-prints (2015), arXiv:1512.04502 [cond-mat.mes-hall].
- [63] M. Ippoliti, S. D. Geraedts, and R. N. Bhatt, *Phys. Rev. B* **96**, 115151 (2017).
- [64] K. Yang, *Phys. Rev. B* **93**, 161302 (2016).
- [65] D. Kamburov, M. A. Mueed, M. Shayegan, L. N. Pfeiffer, K. W. West, K. W. Baldwin, J. J. D. Lee, and R. Winkler, *Phys. Rev. B* **89**, 085304 (2014).
- [66] M. A. Mueed, D. Kamburov, Y. Liu, M. Shayegan, L. N. Pfeiffer, K. W. West, K. W. Baldwin, and R. Winkler, *Phys. Rev. Lett.* **114**, 176805 (2015).
- [67] S. A. Parameswaran, R. Roy, and S. L. Sondhi, *Comptes Rendus Physique* **14**, 816 (2013).
- [68] E. J. Bergholtz and Z. Liu, *International Journal of Modern Physics B* **27**, 1330017 (2013).
- [69] T. Neupert, C. Chamon, T. Iadecola, L. H. Santos, and C. Mudry, *Physica Scripta* **2015**, 014005 (2015).
- [70] E. M. Spanton, A. A. Zibrov, H. Zhou, T. Taniguchi, K. Watanabe, M. P. Zaletel, and A. F. Young, *Science* **360**, 62 (2018).
- [71] H. Bernien, S. Schwartz, A. Keesling, H. Levine, A. Omran, H. Pichler, S. Choi, A. S. Zibrov, M. Endres, M. Greiner, V. Vuletic, and M. D. Lukin, *Nature* **551**, 579 EP (2017), article.
- [72] S. M. Girvin and A. H. MacDonald, “Multicomponent quantum hall systems: The sum of their parts and more,” in *Perspectives in Quantum Hall Effects* (Wiley-Blackwell, 2007) Chap. 5, pp. 161–224.
- [73] J. Eisenstein, *Annual Review of Condensed Matter Physics* **5**, 159 (2014).
- [74] P. Bonderson, A. E. Feiguin, and C. Nayak, *Phys. Rev. Lett.* **106**, 186802 (2011).
- [75] G. Möller, A. Wójs, and N. R. Cooper, *Phys. Rev. Lett.* **107**, 036803 (2011).
- [76] N. Regnault, J. Maciejko, S. A. Kivelson, and S. L. Sondhi, *Phys. Rev. B* **96**, 035150 (2017).
- [77] M. Killi and A. Paramekanti, *Phys. Rev. A* **85**, 061606 (2012).
- [78] M. Killi, S. Trotzky, and A. Paramekanti, *Phys. Rev. A* **86**, 063632 (2012).
- [79] Z. Liu, E. J. Bergholtz, H. Fan, and A. M. Läuchli, *Phys. Rev. Lett.* **109**, 186805 (2012).
- [80] Y.-F. Wang, H. Yao, C.-D. Gong, and D. N. Sheng, *Phys. Rev. B* **86**, 201101 (2012).
- [81] A. Sterdyniak, C. Repellin, B. A. Bernevig, and N. Regnault, *Phys. Rev. B* **87**, 205137 (2013).
- [82] A. Cappelli and E. Randellini, *Journal of High Energy Physics* **2016**, 105 (2016).
- [83] F. Franchini, A. Gromov, M. Kulkarni, and A. Trombettoni, *Journal of Physics A: Mathematical and Theoretical* **48**, 28FT01 (2015).
- [84] F. D. M. Haldane, *Phys. Rev. Lett.* **51**, 605 (1983).
- [85] T. Jolicoeur, *Phys. Rev. B* **95**, 075201 (2017).
- [86] K. Sun, Z. Gu, H. Katsura, and S. Das Sarma, *Phys. Rev. Lett.* **106**, 236803 (2011).
- [87] T. Neupert, L. Santos, C. Chamon, and C. Mudry, *Phys. Rev. Lett.* **106**, 236804 (2011).
- [88] E. Tang, J.-W. Mei, and X.-G. Wen, *Phys. Rev. Lett.* **106**, 236802 (2011).
- [89] T. Langen, R. Geiger, and J. Schmiedmayer, *Annual Review of Condensed Matter Physics* **6**, 201 (2015).
- [90] X. Hu, M. Kargarian, and G. A. Fiete, *Phys. Rev. B* **84**, 155116 (2011).
- [91] Y.-L. Wu, B. A. Bernevig, and N. Regnault, *Phys. Rev. B* **85**, 075116 (2012).
- [92] S. Baier, M. J. Mark, D. Petter, K. Aikawa, L. Chomaz, Z. Cai, M. Baranov, P. Zoller, and F. Ferlaino, *Science* **352**, 201 (2016).
- [93] Y.-L. Wu, N. Regnault, and B. A. Bernevig, *Phys. Rev. Lett.* **110**, 106802 (2013).
- [94] S. A. Parameswaran, R. Roy, and S. L. Sondhi, *Phys. Rev. B* **85**, 241308 (2012).
- [95] B. A. Bernevig and N. Regnault, *Phys. Rev. B* **85**, 075128 (2012).
- [96] C. Repellin, T. Neupert, Z. Papić, and N. Regnault, *Phys. Rev. B* **90**, 045114 (2014).

SUPPLEMENTARY MATERIAL

GEOMETRIC QUENCH IN BIMETRIC THEORY: FURTHER DETAILS

The Lagrangian in the bimetric theory [23] takes the form

$$\mathcal{L} = \frac{\nu\zeta}{2\pi\ell_B^2}\hat{\omega}_0 - \frac{m}{2}\left(\frac{1}{2}\hat{g}^{ij}g_{ij}^m - \gamma\right)^2 \equiv \mathcal{L}_{\text{top}} + \mathcal{L}_{\text{pot}}. \quad (\text{S1})$$

The dynamical degree of freedom here is the vielbein \hat{e}_i^α [51] that “squares” to the dynamic unimodular metric $\hat{g}_{ij} = \hat{e}_i^\alpha \hat{e}_j^\beta \delta_{\alpha\beta}$, or simply $\hat{g} = \hat{e} \cdot \hat{e}^T$. Here \hat{g} corresponds to the intrinsic metric of the FQH state mentioned in the main text. The inverse metric is given by $\hat{G}^{ij} = \hat{E}_\alpha^i \hat{E}_\beta^j \delta^{\alpha\beta}$, where \hat{E}_α^i is the inverse vielbein [51], satisfying $\hat{E}_\alpha^i \hat{e}_j^\alpha = \delta_j^i$. The unimodular condition on \hat{g}_{ij} takes form $\sqrt{\hat{g}} = \sqrt{\hat{g}}$, where $\sqrt{\hat{g}}$ is the determinant of the ambient metric $g_{ij} = \delta_{AB} e_i^A e_j^B$ and e_i^A is the ambient vielbein. Thus, in flat ambient space (that is, when $g_{ij} = \delta_{ij}$), $\sqrt{\hat{g}} = 1$. As explained in the main text, $\hat{\omega}_0$ is the temporal component of the (dynamic) Levi-Civita spin connection, given by

$$\hat{\omega}_0 = \frac{1}{2}\epsilon_{\alpha\beta} \hat{E}_\beta^i \partial_0 \hat{e}_i^\alpha. \quad (\text{S2})$$

The phenomenological coefficient m sets the energy scale which determines the gap of the spin-2 mode. Quantized

coefficient ς is determined by the ‘‘shift’’ \mathcal{S} [23] and takes the value $|\varsigma| = \frac{|\mathcal{S}-1|}{2}$. The phenomenological parameter γ is used to tune the theory close to the nematic phase transition, where the SMA is exact, in the gapped phase $\gamma < 1$. Further details on the bimetric Riemann-Cartan geometry can be found in Refs. [23, 49].

After parameterizing the intrinsic metric \hat{g}_{ij} in terms of Q and ϕ and assuming $g_{ij}^m = \text{diag}[e^A, e^{-A}]$, we have

$$\mathcal{L}_{\text{top}} = \frac{\varsigma \bar{\rho}}{2} (1 - \cosh Q) \dot{\phi} \quad (\text{S3})$$

$$\mathcal{L}_{\text{pot}} = -\frac{m}{2} (\gamma + \sinh A \sinh Q \cos \phi - \cosh A \cosh Q)^2. \quad (\text{S4})$$

The equations of motion are found from

$$\frac{\delta S}{\delta \phi} = 0, \quad \frac{\delta S}{\delta Q} = 0, \quad (\text{S5})$$

where $S = \int d^3x \mathcal{L}$ is the action. The Euler-Lagrange equations yield for the dynamics of \hat{g} the following two equations

$$\begin{aligned} \dot{\phi} \sinh Q &= -2\Omega (\sinh A \cosh Q \cos \phi - \cosh A \sinh Q) \\ &\times (\gamma + \sinh A \sinh Q \cos \phi - \cosh A \cosh Q), \end{aligned} \quad (\text{S6})$$

$$\begin{aligned} \dot{Q} \sinh Q &= -2\Omega \sin \phi \sinh Q \sinh A \\ &(\gamma + \sinh A \sinh Q \cos \phi - \cosh A \cosh Q), \end{aligned} \quad (\text{S7})$$

which were quoted in the main text.

In order to perform the quench, we have to phrase it in terms of Eqs. (S6) and (S7). Taking inspiration from Ref. [83], we perform the quench in two steps. First, we need to fix the initial condition $Q(0), \phi(0)$ for Eqs. (S6) and (S7), which should be determined by the intrinsic metric of the initial Laughlin state $|\psi_0\rangle$. Second, to obtain the quench dynamics, we solve Eqs. (S6) and (S7) under such initial condition, with the value of A determined by the effective anisotropy of H' (or equivalently, by the intrinsic metric of the ground state of H').

In the following, we analyze the solutions of Eqs. (S6) and (S7) in the isotropic limit and what we call ‘‘adiabatic’’ quench regime. The latter refers to the situation where, in equilibrium, the Hamiltonian before and after the quench has the ground state which belongs to the *same* gapped FQH phase.

Isotropic limit

In the isotropic case we must take $A \rightarrow 0$. We find

$$\dot{Q} = 0, \quad \dot{\phi} = 2\Omega (\gamma - \cosh Q). \quad (\text{S8})$$

Choosing the solution $Q = 0$ of the first equation, the second equation reads

$$\dot{\phi} = -2\Omega(1-\gamma) \equiv -E_\gamma \quad \Rightarrow \quad \phi(t) = \phi(0) - E_\gamma t, \quad (\text{S9})$$

from where we interpret $E_\gamma = 2\Omega(1-\gamma) = \frac{2m(1-\gamma)}{\bar{\rho}\varsigma}$ as the gap of the spin-2 part of the GMP mode at $\mathbf{k} = 0$ [23]. When $\gamma \rightarrow 1$, the gap closes and the FQH state undergoes a nematic phase transition [23]. The dynamical metric evaluated on this solution takes the form

$$\hat{g}_{ij} = \begin{pmatrix} 1 & 0 \\ 0 & 1 \end{pmatrix}, \quad (\text{S10})$$

consequently the dynamics of $\phi(t)$ is not visible in the fluctuations of the dynamical metric. Formally speaking, this happens because $Q = 0$. When Q is different from 0, the metric will be sensitive to the dynamics of ϕ . This is what happens in the case of sufficiently weak anisotropy which is discussed next.

Adiabatic quench regime

When anisotropy is weak (i.e., the corresponding equilibrium ground state is in the gapped FQH phase), we can assume both A and Q are close to 0. Taylor expansion of Eqs. (S6) and (S7) in A and Q leads to the following system of linear equations

$$\dot{\phi} Q = E_\gamma (A \cos \phi - Q), \quad (\text{S11})$$

$$\dot{Q} = E_\gamma A \sin \phi. \quad (\text{S12})$$

Analytical solutions for this system of equations exist under suitable initial conditions. In particular, for $Q(0) = 0$, it can be verified by direct substitution that

$$Q(t) = \pm 2A \sin\left(\frac{E_\gamma t}{2}\right), \quad \phi(t) = \pi \mp \frac{\pi}{2} - \frac{E_\gamma t}{2}. \quad (\text{S13})$$

are exact solutions. These are exactly the equations from the main text which were used to fit the numerical data.

As long as the quench is adiabatic, the linearized Eqs. (S11) and (S12) provide a very accurate approximation to the full non-linear dynamics. Fig. S1 shows the comparison of the numerical solutions of non-linear Eqs. (S6) and (S7) satisfying $Q(0) = 0$ against their linearized counterparts, Eq. (S13), where we focus on the $Q \geq 0$ part and consider $\phi \bmod 2\pi$. Red solid lines in Fig. S1 result from a combination of the \pm branches in Eq. (S13), which gives us Q and ϕ as periodic functions with frequency E_γ . Mathematically, it is curious that Eq. (S13) display such close agreement with the solutions of Eqs. (S6) and (S7), since the latter appear to be complicated non-linear equations.

GENERALIZED PSEUDOPOTENTIALS

In Ref. [50] it was shown that any two-particle interaction, including cases where metrics g_m and g_i are different, can be expanded into an orthonormal basis of generalized pseudopotentials. These operators maintain translation invariance, but break rotation symmetry down to

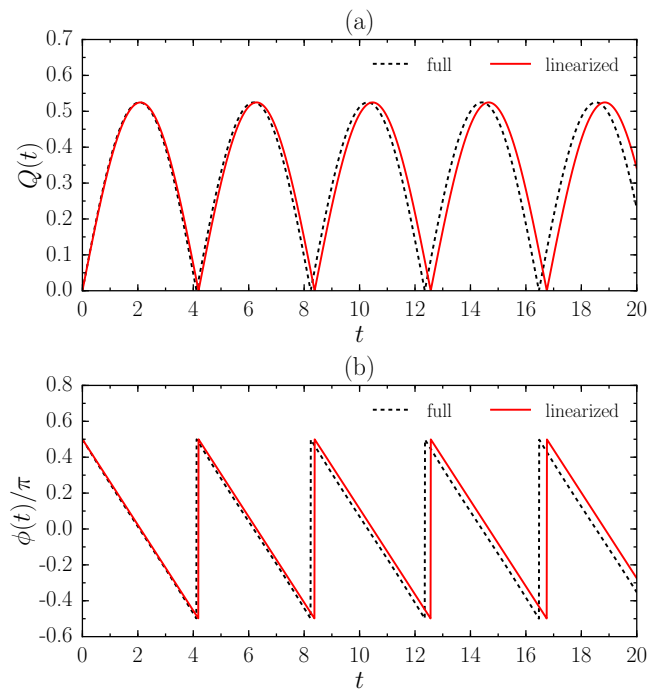


FIG. S1. Predictions of the bimetric theory for (a) Q and (b) ϕ under the initial condition $Q(0) = 0$. Black dashed lines indicate the numerical solution of the full equations, Eqs. (S6) and (S7). Red solid lines indicate the analytical solution Eq. (S13) of the linearized system, Eqs. (S11) and (S12). Here we focus on the $Q \geq 0$ solution. The parameters are fixed at $\Omega = 1.5/4$, $\gamma = -1$, $A = \ln 1.3$.

a discrete subgroup. Up to normalization prefactors, the generalized pseudopotentials are given by [50]

$$V_{m,n}(g_p; q_x, q_y) = L_m^n(g_p^{ab} q_a q_b) \mathbf{q}^n + c.c., \quad (\text{S14})$$

where m, n are even integers (for bosons). When $n = 0$, these reduce to the usual (isotropic) Haldane pseudopotentials [84]. $V_{m,n}$ explicitly depends on the metric g_p through the argument of the Laguerre polynomial, as well as the vector \mathbf{q} . For simplicity, we fix $g_p = \mathbb{1}$ and $\mathbf{q} = \frac{1}{\sqrt{2}}(q_x + iq_y)$ in our numerics.

Contours of leading-order $V_{m,n}$ for bosons are depicted in Fig. S2. In particular, we can observe that $V_{0,2}$ has a clear quadrupolar structure in momentum space, indicating that $\hat{V}_{0,2}$ carries angular momentum $L_z = 2$. Unlike $V_{0,2}$, $V_{0,4}$ has an octupolar structure, which implies that it would couple the ground state to higher-spin excitations. In our case, this is a spin-4 excitation because the odd-spin ones vanish due to inversion symmetry, which is a generic symmetry of LLL-projected FQH Hamiltonians.

Since $\hat{V}_{0,2}$ and $\hat{V}_{0,4}$ may couple to excitations with different spins, we expect that adding a small amount of them to pure \hat{V}_0 will lead to completely different quench dynamics. Since $\hat{V}_{0,2}$ carries angular momentum $L_z = 2$, its presence should drive a quench dominated by the spin-

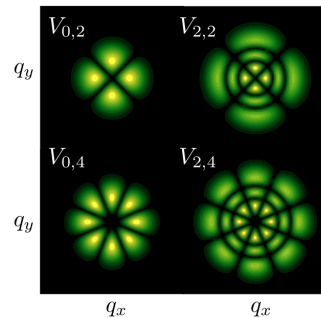


FIG. S2. Contours in momentum space of the leading order anisotropic pseudopotentials for bosons [50] with quadrupolar ($V_{0,2}, V_{2,2}$) and octupolar ($V_{0,4}, V_{2,4}$) structure.

2 mode. Indeed, we find that the consequent exact dynamics of \hat{g} behaves according to the description based on spin-2 graviton oscillation (Fig. S3), and is very similar to that obtained by changing the mass tensor in the main text. However, when driving the quench by adding a small amount of $\hat{V}_{0,4}$ we find $Q(t) \equiv 0$ during the entire measured time interval (see the black solid line in Fig. S3). This suggests that the spin-2 collective mode is not excited in this case, and the quench is dominated by spin-4 collective modes. Thus, we see that only the simplest type of geometric quench (driven by $\hat{V}_{0,2}$) corresponds to the picture of the graviton oscillation, which can be analytically described in the framework of the bimetric theory. More complicated types of quenches, such as the one driven by $\hat{V}_{0,4}$, give rise to richer types of dynamics, as discussed in the main text, which cannot be modelled in the existing formalism of the bimetric theory.

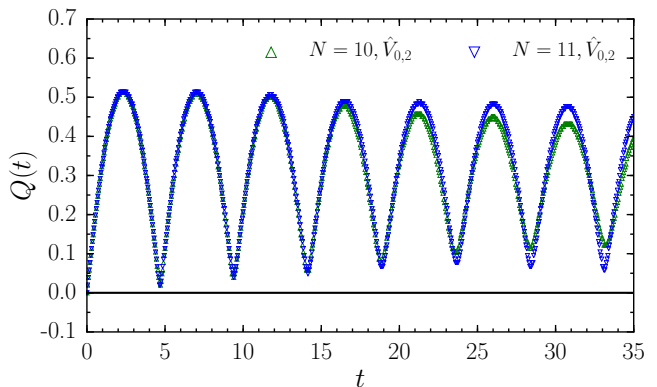


FIG. S3. Exact dynamics of Q for the quench with $\hat{V}_0 \rightarrow \hat{V}_0 + 0.1\hat{V}_{0,2}$ (color symbol) and $\hat{V}_0 \rightarrow \hat{V}_0 + 0.1\hat{V}_{0,4}$ (black solid line). A complete absence of dynamics of \hat{g} can be noticed in the case of the perturbation by $\hat{V}_{0,4}$.

GEOMETRIC QUENCH OF $\nu = 1/2$ BOSONS: COULOMB INTERACTION

In the main text, we have focused on the geometric quench of $\nu = 1/2$ bosons interacting via contact interaction. Here we show that the picture of graviton oscillation also holds for Coulomb interacting bosons.

For Coulomb interacting bosons, the difference is that we have two extrinsic metrics in the problem: the Landau orbit metric g_m , which was used to drive the quench in the main text, and also the Coulomb metric g_i . We choose to keep g_i isotropic, i.e., we fix $V_{\mathbf{q}} = 2\pi/\sqrt{q_x^2 + q_y^2}$, and we change the mass tensor g_m to drive the quench. For the time being, we still focus on adiabatic isotropic-to-anisotropic geometric quench by choosing $A_0 = 0$ and $A_1 = \ln 2.0$. In this case, the initial state is the isotropic Coulomb ground state, which is well approximated by the isotropic Laughlin model state.

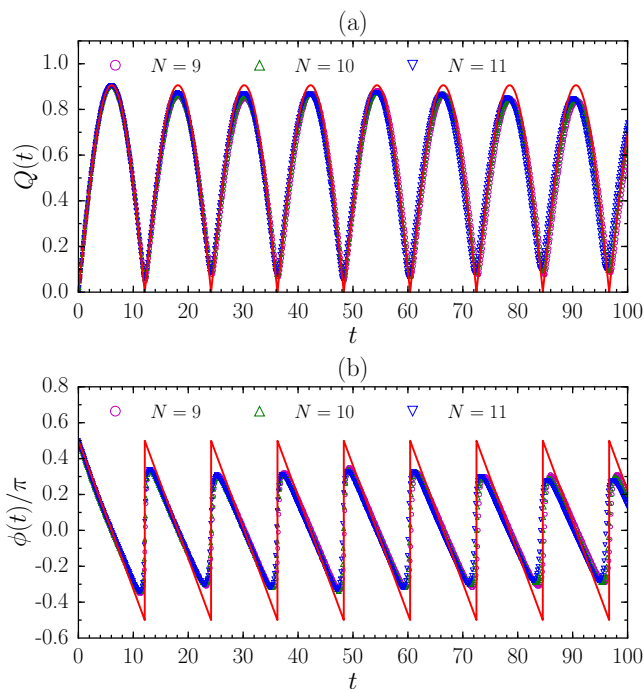


FIG. S4. Exact dynamics of (a) Q and (b) ϕ for $N = 9 - 11$ bosons at $\nu = 1/2$ with the Coulomb interaction. The quench is driven by choosing $A_0 = 0$ and $A_1 = \ln 2.0$. The red curves are fits to Eq. (S13), which coincide with the predictions of the bimetric theory.

Exact dynamics of \hat{g} up to moderate times is shown in Fig. S4. Similar to results in the main text, both Q and ϕ again oscillate with a well-defined frequency. Fitting the first one or two oscillations in Fig. S4 against Eq. (S13) yields a remarkably accurate agreement with full dynamics across the entire time interval, suggesting the validity of the bimetric theory also in this case. The fit gives the frequency $E_\gamma \approx 0.520$, which is expected to match

the graviton gap of the Coulomb interaction. Indeed, we observe a pronounced peak in the spectral function of $\hat{V}_{0,2}$ for the Coulomb interaction, which probes the graviton mode and estimates the graviton gap as 0.55 (Fig. S5). Note that the Fourier transform of Q has a pronounced peak at the same energy, which further confirms that the dynamics is dominated by the graviton mode. Moreover, the effective anisotropy in the quench Hamiltonian is expected to be weaker than g'_m because we keep isotropic g_i and only change g_m . Indeed, the value of A returned by the fitting is $A \approx 0.454$, which is between 0 and $A_1 = \ln 2.0 \approx 0.693$.

In summary, our numerical results demonstrate that the dynamics following the weak geometric quench of Coulomb interacting bosons are also graviton oscillations which fall under the description of the bimetric theory. Comparing the results for Coulomb interaction with those for contact interaction in the main text, we observe, somewhat surprisingly, that the spectral function is “sharper” in the Coulomb case. This reflects the fact that the $k \rightarrow 0$ limit of the SMA excitation is closer to the threshold of the two-roton continuum in the Coulomb case. While similar result is numerically found for fermions in the higher Landau level ($\nu = 7/3$) with Coulomb interaction [85], it is presently not clear how different interactions affect the position of the $k \rightarrow 0$ limit of the SMA mode.

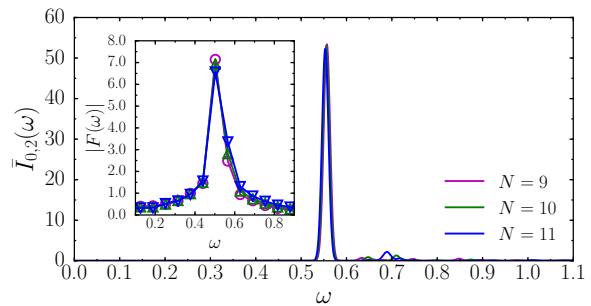


FIG. S5. Normalized spectral function $\bar{I}_{0,2}(\omega)$ for isotropic systems of $N = 9 - 11$ bosons at $\nu = 1/2$ with Coulomb interactions. Inset shows the discrete Fourier transform $|F(\omega)|$ of Q in Fig. S4. Markers in the inset and curves in the main figure with the same color refer to the same system size.

GENERALIZATIONS OF THE QUENCH PROTOCOL

In the main text, we have presented results for the simplest type of quench where the initial state is isotropic and the Hamiltonian is instantaneously made (weakly) anisotropic. Here we consider two direct generalizations of such protocols: when the initial state is itself anisotropic, and when the quench is introduced over some finite amount of time.

Anisotropic-to-anisotropic quench

As an immediate generalization of the isotropic-to-anisotropic quench, we now discuss the more general case of a quench with $A_1 > A_0 > 0$, for which the initial state is already anisotropic. Interestingly, after this simple modification, we have not been able to find analytical solutions under the general initial conditions $Q(0) > 0, \phi(0) = 0$, even for the linearized systems Eqs. (S11) and (S12). However, we can still numerically solve the system of coupled differential equations, and we find that the bimetric theory continues to accurately describe the short-time dynamics of Q and ϕ , and also captures the oscillatory dynamics very well up to moderate times.

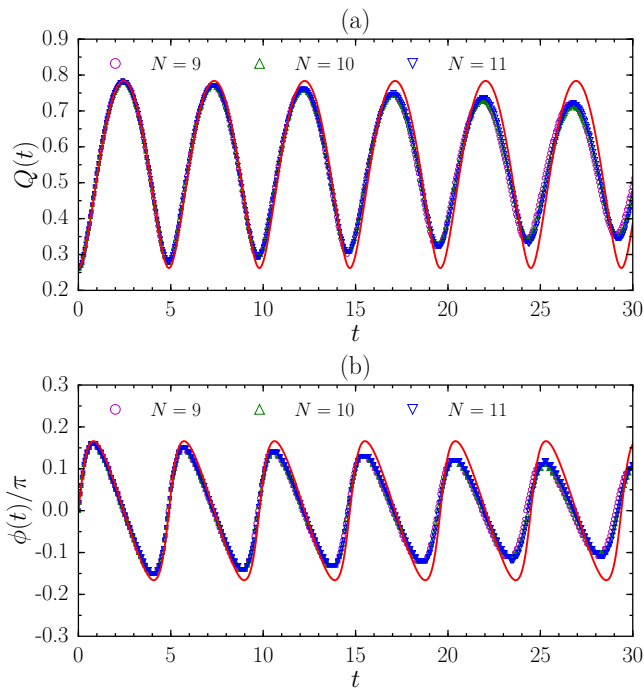


FIG. S6. Exact dynamics of (a) Q and (b) ϕ for $N = 9 - 11$ bosons at $\nu = 1/2$ with the contact interaction. The weak geometric quench is driven by choosing $A_0 = \ln 1.3$ and $A_1 = \ln 1.7$. The red solid curve is the solution of linearized equations Eqs. (S11) and (S12) under the initial condition $Q(0) = A_0, \phi(0) = 0$, with $A \approx 0.523$ and $E_\gamma \approx 1.283$. These two parameters are obtained by fitting the first oscillation of Q of $N = 11$ against the solution.

To illustrate this, in Fig. S6, we choose $A_0 = \ln 1.3$ and $A_1 = \ln 1.7$, and show the exact dynamics for the quench driven by the contact interaction. Since the initial state is a Laughlin model state with $\hat{g}(0) = g_m$, the bimetric theory predicts the post-quench dynamics of \hat{g} is governed by the solution of Eqs. (S11) and (S12) with initial condition $Q(0) = A_0, \phi(0) = 0$. Indeed, the numerical data in the first two periods again lie on top of such a solution with fitting parameters $A \approx 0.523$ and $E_\gamma \approx 1.283$. The

value of A is close to $A_1 = \ln 1.7 \approx 0.531$, as expected, and $E_\gamma \approx 1.283$ is consistent with the graviton gap estimated from both the $I_{0,2}(\omega)$ spectral function and the numerical results of isotropic-to-anisotropic quench.

As discussed in the main text, apart from generally good agreement, we can also observe some discrepancy between the exact dynamics and the equations of the bimetric theory in Fig. S6. This discrepancy is likely caused by the mentioned finite-size effect (the splitting of the spin-2 mode into several states and the Lieb-Robinson light cone) and the possible contribution of higher-spin modes. Compared to isotropic-to-anisotropic quench, stronger finite-size effects in the present case could be anticipated due to anisotropy effectively reducing the length of the system along one of the spatial directions.

Non-instantaneous quench

Instantaneous quench is the minimal theoretical model that describes sudden tilt of the magnetic field. However, since any experimental manipulation takes finite time, it is natural to ask how our results generalize to more realistic, non-instantaneous quenches.

To be specific, we consider isotropic-to-anisotropic quenches driven by a time-dependent ramp of the mass tensor, i.e., $g_m = \text{diag}(e^{A(t)}, e^{-A(t)})$ with

$$A(t) = A_1 \exp(-t_0/t), \quad (\text{S15})$$

such that $A(0) = 0$ and $A(+\infty) = A_1$. The slope of the ramp depends on some characteristic time, t_0 . When $t_0 = 0$, we recover the instantaneous quench. We thus expect that differences between the non-instantaneous quench and the instantaneous one are negligible when t_0 is small, while some qualitative changes may happen for large enough t_0 .

As a representative example, we choose $A_1 = \ln 1.3$ (which we expect to be adiabatic) and show the predicted behavior of Q and ϕ in the bimetric theory, i.e., the solutions of the full equations [Eqs. (S6) and (S7)], for different t_0 in Fig. S7. We indeed find that the solutions in the non-instantaneous case agree with their instantaneous limit up to $t_0 \lesssim 10^{-2}$. The effect of the ramp starts to appear when $t_0 \sim 10^{-1}$, which leads to gradual deviations of both the amplitude and frequency in the dynamics from the instantaneous case. Finally, for very large $t_0 \gtrsim 1$, we observe strongly distorted oscillation patterns in Q and ϕ , revealing very different dynamics between the fast-quench and slow-quench regimes.

It would be interesting to compare exact dynamics of finite systems with the predictions of the bimetric theory also for non-instantaneous quenches, as we have done for the instantaneous case. Due to the time-dependent nature of the non-instantaneous quench, the many-body numerical simulation in this case is more complicated and will be presented in future work. However, because the

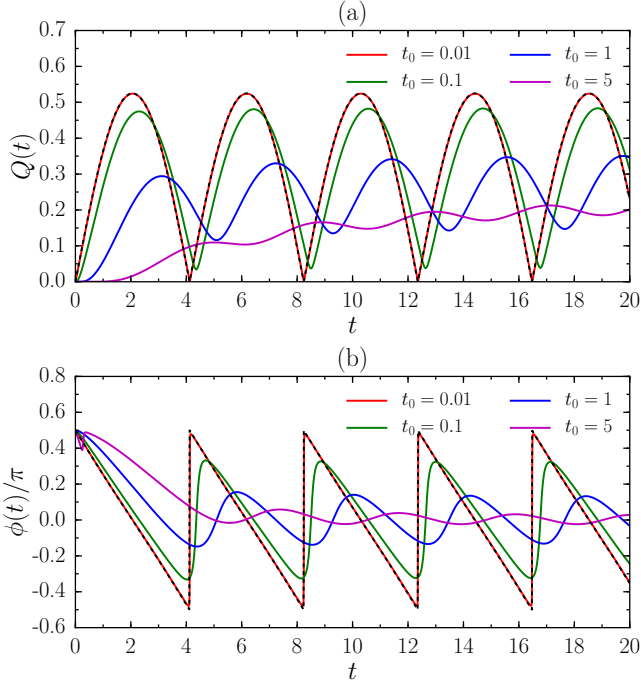


FIG. S7. Solutions of the full equations [Eqs. (S6) and (S7)] for the non-instantaneous quench with $A(t) = A_1 \exp(-t_0/t)$, under the initial condition $Q(0) = 0$. Here we focus on the $Q \geq 0$ solution. We choose $\Omega = 1.5/4$, $\gamma = -1$, $A_1 = \ln 1.3$, and consider several different $t_0 = 0.01, 0.1, 1$ and 5 . For comparison, we also give solutions for the instantaneous quench as black dashed lines.

instantaneous quench corresponds to a stronger perturbation of the system, we expect similar or better agreement between theory and numerics for the case of non-instantaneous quenches.

PROJECTED DYNAMICS

The main premise of the bimetric theory is the existence of a single spin-2 degree of freedom which can be excited by changing the system's anisotropy. However, this is an effective description of a FQH system, and it is not *a priori* clear whether this degree of freedom is represented by a *single* many-body eigenstate or several of them which span a range of energies. In the latter case, we may expect the oscillations to decay due to dephasing between different eigenstates that are associated with the effective spin-2 degree of freedom. Here we scrutinize this conjecture by quantifying how well the full dynamics of a FQH system of bosons can be reproduced by an explicit projection to the subset of eigenstates centered around the the energy of the spin-2 mode.

The projected subspace is defined by the eigenstates $|n\rangle$ of the quench Hamiltonian H' with dominant matrix elements $|\langle n|\hat{V}_{0,2}|0\rangle|^2$. The weight of this projection is

measured by

$$f = \left(\sum_{n=0}^{M-1} |\langle n|\hat{V}_{0,2}|0\rangle|^2 \right) / \left(\sum_{n=0}^{D-1} |\langle n|\hat{V}_{0,2}|0\rangle|^2 \right), \quad (\text{S16})$$

where $|n\rangle$ have been sorted in descending order according to $|\langle n|\hat{V}_{0,2}|0\rangle|^2$. Here M is the number of kept states and D is the total number of eigenstates that we can obtain from exact diagonalization of H' , i.e., D is equal to the Hilbert space dimension in the $\mathbf{k} = 0$ sector for $N \leq 9$, while for practical reasons we kept $D = 200$ for larger systems ($N = 10 - 12$). Remarkably, the number of states we need to saturate the total weight f is significantly smaller than the Hilbert space dimension. Fixing $f = 99\%$, the finite-size scaling of the required M clearly indicates that only an exponentially small fraction of the whole Hilbert space carries spin-2, as seen in Fig. S8.

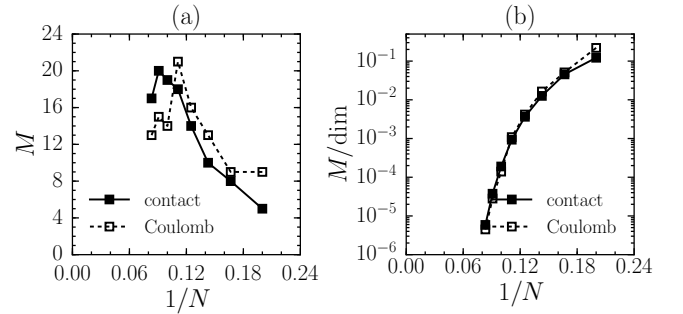


FIG. S8. Finite-size scaling of the number of spin-2 states in the $\mathbf{k} = 0$ Hilbert space for $N = 5 - 12$ bosons at $\nu = 1/2$. M represents the number of states which contain $f = 99\%$ of the total $|\langle n|\hat{V}_{0,2}|0\rangle|^2$. We consider both contact and Coulomb quench Hamiltonians, with $A_1 = \ln 1.3$ and $A_1 = \ln 2.0$, respectively. The plots show (a) M and (b) M/dim , where dim is the $\mathbf{k} = 0$ Hilbert space dimension.

While the exponentially decaying ratio of M to the Hilbert space dimension might not be entirely surprising (since it still does not preclude M being exponentially large in the system size), it can also be shown that, in absolute terms, only a very small number of states M yields a very accurate approximation to the exact dynamics. We perform the projection explicitly, i.e., we calculate the post-quench state as $|\tilde{\psi}(t)\rangle = \frac{1}{\mathcal{N}} \sum_{n \in \mathcal{S}} \exp(-i\epsilon_n t) \langle n|\psi_0\rangle |n\rangle$, where \mathcal{S} contains the first M eigenstates with the largest $|\langle n|\hat{V}_{0,2}|0\rangle|^2$ matrix elements and \mathcal{N} is the normalization factor. The dynamics of the intrinsic metric of $|\tilde{\psi}(t)\rangle$ after an isotropic-anisotropic quench is shown in Fig. S9 for $N = 11$ bosons, together with exact dynamics without the projection. As expected, the projected dynamics approaches the exact dynamics with increasing M . However, for both contact and Coulomb interactions, the main feature in exact dynamics has been accurately reproduced by M less than 10, even if there are as many as 533160 eigenstates in the entire $\mathbf{k} = 0$ Hilbert space, which is more than four

orders of magnitude larger. Such an excellent approximation of the exact dynamics by a tiny spin-2 fraction of the whole Hilbert space is a compelling evidence for the picture of graviton oscillation and the bimetric theory.

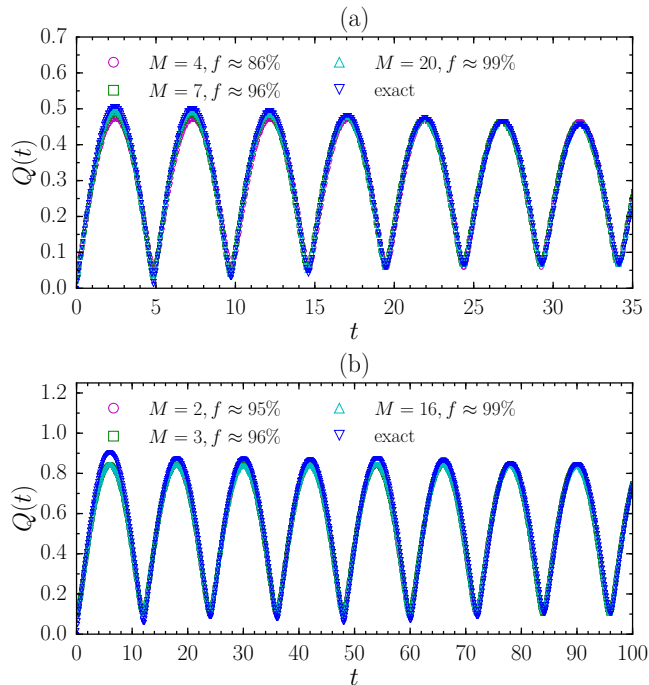


FIG. S9. Dynamics of Q projected to M eigenstates of H' with dominant $|\langle n|\hat{V}_{0,2}|0\rangle|^2$. We consider $N = 11$ bosons at $\nu = 1/2$ with (a) contact and (b) Coulomb interactions. The quench parameters A_0 and A_1 are the same as those used in the main text and in Fig. S4, respectively.

GEOMETRIC QUENCH OF $\nu = 1/3$ FERMIONS

All our results presented in the main text and up to this point have been for bosons at filling fraction $\nu = 1/2$, which is the most fundamental of all FQH phases. In actual experimental systems, FQH effect is of course mainly studied with electrons as charge carriers. Now we demonstrate that our results directly apply to the case of fermions at filling factor $\nu = 1/3$ as well, with somewhat stronger finite-size effects.

Similar to bosons, we consider two types of interactions for fermions. In the first case, we assume model (short-range) V_1 interaction with $V_{\mathbf{q}} = L_1(g_i^{ab}q_aq_b)$ (L_1 is the first Laguerre polynomial), for which the $\nu = 1/3$ Laughlin state is the unique (and the densest) zero-energy state [84]. As customary in the literature [22], we assume $g_i = g_m$ for the model interaction when driving the quench. In the second case, we consider Coulomb interaction, for which g_i is kept isotropic, i.e., $V_{\mathbf{q}} = 2\pi/\sqrt{q_x^2 + q_y^2}$, but g_m is allowed to be non-isotropic. As

representative examples, we focus on adiabatic isotropic-anisotropic quenches with $A_0 = 0$ and $A_1 > 0$, where we choose $A_1 = \ln 1.3$ and $A_1 = \ln 2.0$ for quenches driven by V_1 and Coulomb interactions, respectively. Exact dynamics of \hat{g} up to moderate times is shown in Figs. S10 and S11 for these two types of interactions.

Similar to $\nu = 1/2$ bosons, the short-time dynamics of adiabatic quenches for $\nu = 1/3$ fermions fully agrees with the bimetric theory. We can thus extract parameters A and E_γ by fitting the numerical data against Eq. (S13), whose values are given in the captions of Figs. S10 and S11. The value of A , which quantifies the anisotropy in the interaction, is again close to A_1 (between 0 and A_1) for the V_1 (Coulomb) interaction as expected. The value of E_γ estimates the graviton gap as 1.46 and 0.14 for V_1 and Coulomb interactions, respectively, matching the values given by the $\hat{V}_{1,2}$ spectral function (not shown here). Note that the graviton gap of the Coulomb interaction that we extract from the quench dynamics precisely matches the value given by other methods in the context of single-mode approximation [7, 54].

Like in the bosonic case, we also observe deviations from the bimetric theory at longer times for $\nu = 1/3$ fermions. However, these deviations are more pronounced and appear at earlier times than those for $\nu = 1/2$ bosons. For quenches driven by the V_1 interaction, while the overall oscillation structure is maintained up to moderate times, the oscillation amplitude already visibly decays after the first oscillation (Fig. S10). The situation is even more pronounced for quenches driven by the Coulomb interaction, as expected. In that case, the behavior of Q and ϕ totally departs from simple oscillations after the first period and the curves of different system sizes are no longer on top of each other (Fig. S11). Compared with $\nu = 1/2$ bosons, our numerical results clearly demonstrate that the dynamics of $\nu = 1/3$ fermions suffers more from finite-size effects, and larger systems are needed to obtain fully converged dynamical evolution.

GEOMETRIC QUENCH FOR FRACTIONAL CHERN INSULATORS

Here we generalize the geometric quench from continuum FQH states to their lattice analogs – the fractional Chern insulators (FCIs) [67–69]. Contrary to conventional FQH states, FCIs do not require an external magnetic field [86, 87] and may potentially persist at higher temperatures [88]. Considering the recent experimental progress on quantum many-body dynamics in optical lattices [89], FCIs realized by cold atoms in optical lattices could be a promising platform to observe the dynamics after a geometric quench on much longer time scales than possible in semiconductor FQH systems. In the following, we propose a quench protocol for FCIs and demonstrate that our main results directly apply to this type of sys-

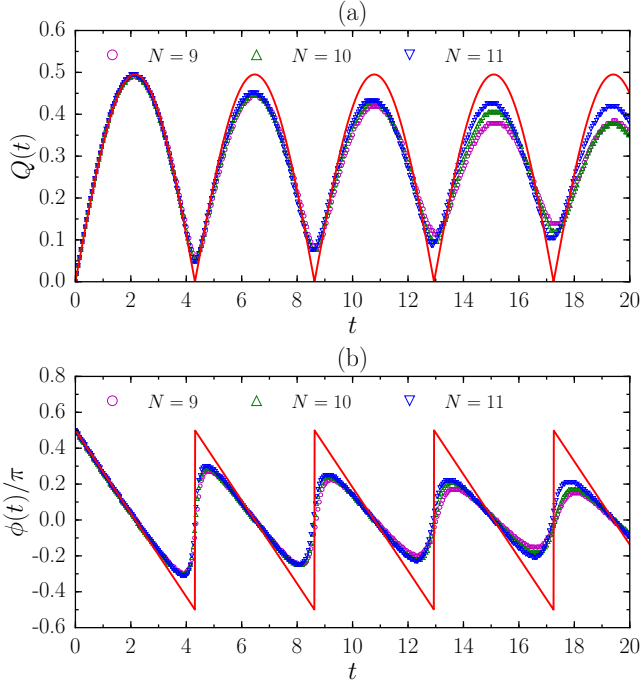


FIG. S10. Exact dynamics of (a) Q and (b) ϕ for $N = 9 - 11$ fermions at $\nu = 1/3$ with the V_1 interaction. The weak geometric quench is driven by choosing $A_0 = 0$ and $A_1 = \ln 1.3$. The red solid curve is the $Q \geq 0$ part of Eq. (S13), with $A \approx 0.248$ and $E_\gamma \approx 1.457$. These two parameters are obtained by fitting the first oscillation of Q of $N = 11$ against the solution.

tem. As FCIs are inherently anisotropic, the quenches in FCI belong to the anisotropic-to-anisotropic case.

For concreteness, we consider N bosons in a two-dimensional Ruby lattice [90] of $N_1 \times N_2$ unit cells. The system is in $x - y$ plane with periodic boundary conditions. We adopt the same tight-binding parameters and lattice configurations as in Ref. [91], for which the lowest Bloch band is flat and has Chern number $C = 1$. We assume that bosons interact via onsite and dipolar potentials. If all dipoles are polarized in xz plane with an angle α to the $+z$ direction, the interaction Hamiltonian can be written as

$$H_{\text{int}} = \sum_i n_i(n_i - 1) + \sum_{i < j} \frac{r_{ij}^2 - 3x_{ij}^2 \sin^2 \alpha}{r_{ij}^5} n_i n_j, \quad (\text{S17})$$

where n_i is the occupation on lattice site i , and $r_{ij} = (x_{ij}, y_{ij})$ is the distance between lattice site i and j . We project the interaction to the lowest band and verify that the ground state at band filling $\nu = N/(N_1 N_2) = 1/2$ is the $\nu = 1/2$ bosonic Laughlin FCI for a finite range of α , characterized by a robust two-fold topological degeneracy. In order to keep the lattice aspect ratio close to 1 and for the two degenerate FCI states to be located in differ-

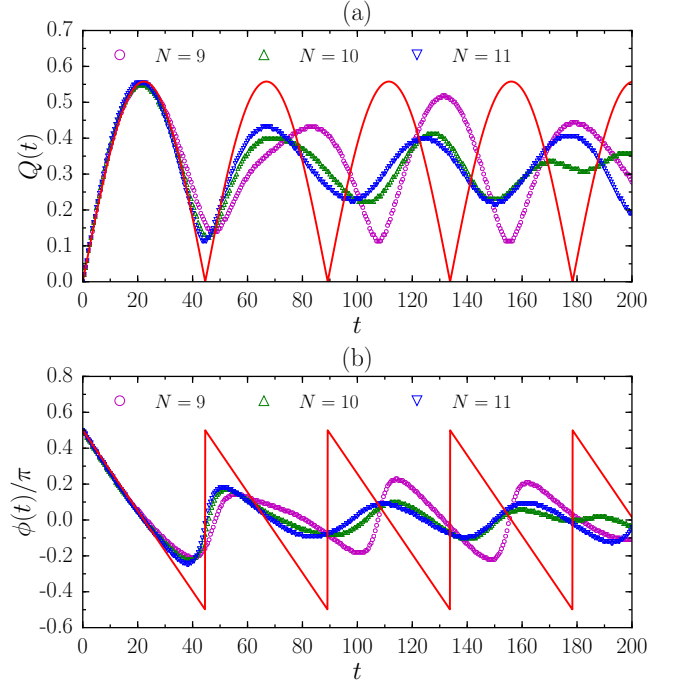


FIG. S11. Exact dynamics of (a) Q and (b) ϕ for $N = 9 - 11$ fermions at $\nu = 1/3$ with the Coulomb interaction. The weak geometric quench is driven by choosing $A_0 = 0$ and $A_1 = \ln 2.0$. The red solid curve is the $Q \geq 0$ part of Eq. (S13), with $A \approx 0.279$ and $E_\gamma \approx 0.141$. These two parameters are obtained by fitting the first oscillation of Q of $N = 11$ against the solution.

ent momentum sectors, we focus on two system sizes below: $N = 6, N_1 = 3, N_2 = 4$ and $N = 10, N_1 = 4, N_2 = 5$.

While the interaction is isotropic for $\alpha = 0$, tuning α away from 0 adds anisotropy, which can be experimentally achieved by changing the direction of the polarizing magnetic field [92]. We prepare the initial state as the ground state with momentum $\mathbf{K} = \mathbf{0}$, then drive the quench by suddenly changing α from 0 to a small but finite α' (adiabatic quench). Tuning α is not a direct lattice analogue of changing the geometry of continuum Landau level orbitals, but it is also expected to excite a geometric degree of freedom in FCIs because it adds quadrupolar anisotropy to the system. In order to confirm this, we track the dynamics of fidelity $|\langle \psi(t) | \psi(0) \rangle|^2$, and compare its dominant frequency with the energy of the FCI graviton mode. The latter can be probed by a suitable lattice analogue of the $\hat{V}_{0,2}$ pseudopotential. A detailed study of intrinsic metric is also feasible for FCIs by the FCI-FQH mapping [93] and will be presented in future work.

In Fig. S12, we show the fidelity and its discrete Fourier transform for $\alpha' = 15^\circ$. One can see that the dynamics of fidelity is dominated by a single frequency, characterized by the pronounced peak at $\omega \approx 0.47$ in the discrete Fourier transform [Fig. S12(b)]. In order to estimate the

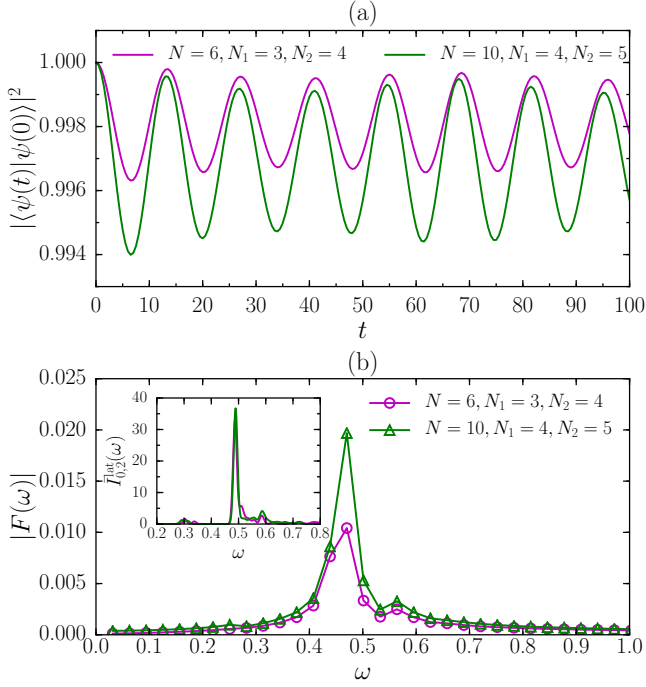


FIG. S12. (a) Dynamics of fidelity, $|\langle \psi(t) | \psi(0) \rangle|^2$, and (b) its discrete Fourier transform for $\nu = 1/2$ bosonic Laughlin FCIs. The weak quench is driven by $\alpha' = 15^\circ$. The inset of (b) shows the normalized spectral function $\bar{I}_{0,2}^{\text{lat}}(\omega) = I_{0,2}^{\text{lat}}(\omega) / \int I_{0,2}^{\text{lat}}(\omega) d\omega$ for the isotropic case with $\alpha = 0$. Markers in insets and curves in main figures with the same color refer to the same system size.

graviton energy on the lattice, we define the operator

$$\hat{V}_{0,2}^{\text{lat}} = \sum_{\mathbf{q}} (\cos q_1 - \cos q_2) \bar{\rho}_{\mathbf{q}}^{\text{lat}} \bar{\rho}_{-\mathbf{q}}^{\text{lat}}, \quad (\text{S18})$$

where $q_i = \mathbf{q} \cdot \mathbf{b}_i$ with \mathbf{b}_i 's the two basic lattice direction vectors, \mathbf{q} is in the first Brillouin zone, and $\bar{\rho}_{\mathbf{q}}^{\text{lat}}$ is the density operator $e^{i\mathbf{q} \cdot \hat{\mathbf{r}}}$ projected to the lowest Bloch band (see Refs. [93–96] for the explicit form of $\bar{\rho}_{\mathbf{q}}^{\text{lat}}$). Similar to the continuum $\hat{V}_{0,2}$ pseudopotential, $\hat{V}_{0,2}^{\text{lat}}$ effectively carries angular momentum $L_z = 2$ to probe spin-2 states on the lattice, because the \mathbf{q} -dependence term $\cos q_1 - \cos q_2$ takes a d -wave form $q_1^2 - q_2^2$ at small $|\mathbf{q}|$. Indeed, its spectral function

$$I_{0,2}^{\text{lat}}(\omega) = \sum_j \delta(\omega - \epsilon_j) |\langle j | \hat{V}_{0,2}^{\text{lat}} | 0 \rangle|^2 \quad (\text{S19})$$

shows sharply pronounced peaks [inset of Fig. S12(b)], where ϵ_j and $|j\rangle$ are the eigen-energy and eigenstate of the projected interaction Eq. (S17). Since these peaks appear around the same energy as that in the discrete Fourier transform of fidelity, our quench protocol indeed excites the geometric degree of freedom of FCI that corresponds to the spin-2 graviton mode on a lattice. The similarity of the FCI results to the continuum FQH is rather surprising, in light of the fact that there are no quantitative arguments that support the relation between the bimetric theory and FCIs (beyond the intuitive arguments mentioned in Ref. [23]).